Eur. Phys. J. D **28**, 351–360 (2004)
DOI: 10.1140/epjd/e2004-00001-y

THE EUROPEAN PHYSICAL JOURNAL D

Accurate asymptotic ground state potential curves of Cs_2 from two-colour photoassociation

N. Vanhaecke, Ch. Lisdat, B. T'Jampens, D. Comparat, A. Crubellier, and P. Pillet[a]

Laboratoire Aimé Cotton, CNRS, bâtiment 505, Campus d'Orsay, 91405 Orsay Cedex, France

Received 17 July 2003 / Received in final form 4 November 2003
Published online 20 January 2004

Abstract. Over 100 high lying level energies of the lowest electronic states $X^1\Sigma_g^+$ and $a^3\Sigma_u^+$ in Cs_2 are determined in a Λ-like scheme two-colour photoassociation spectroscopy. The results are analyzed with a coupled channel model using an asymptotic approach, based on nodal lines. From this analysis we determine the long range dispersion coefficient C_6 to 6846.2±15.6 a.u. We also obtain the first experimental determination of the amplitude of the asymptotic exchange term.

PACS. 34.20.-b Interatomic and intermolecular potentials and forces, potential energy surfaces for collisions – 32.80.Pj Optical cooling of atoms; trapping – 03.65.Ge Solutions of wave equations: bound states

1 Introduction

Over the last decade, the development of laser cooling and trapping techniques made the study of interactions inside ultracold dilute gases possible. This has led to the observation of Bose-Einstein condensation in atomic gases and it has also resulted in a large survey of two-body interactions. Ultracold atomic samples are powerful tools to probe collisional properties [1] as well as to investigate molecular states [2,3]. At ultracold temperatures achieved in magneto-optical traps, a single parameter, the s-wave scattering length characterizes entirely elastic two-body interactions. This quantity images the whole two-body interaction potential, and is very sensitive to its asymptotic part, which is also crucial for the binding energy of the most weakly bound levels of the ground state potentials.

Photoassociation (PA) in cold atomic samples provides a high resolution spectroscopic method which enables precise study, e.g. of the first electronically excited states in alkali dimers [4]. PA spectroscopy offers a novel method to analyze long-range molecules [5], that are quite difficult to reach by standard ways [6,7]. PA has also led to cold molecule formation [8]. Measurements of PA cross-sections enabled the derivation of collision wavefunctions, extrapolated to zero-energy to evaluate the scattering length [9,10]. Multi-photon processes have also been applied in cold atomic samples in ladder-like [11] and Λ-like schemes [12–14]. A useful theoretical treatment of one and two-colour photoassociative spectroscopy has been presented in [15,16]. The richness of two-colour lineshapes (Fano profiles, optical Feshbach resonances) has been demonstrated in Cs experiment [17].

We have measured and analyzed the energies of more than 100 high lying levels of the lowest electronic states of Cs_2. In these levels, which are very close to the dissociation thresholds, the two nuclei spent most of the time at large internuclear distances, in the so-called asymptotic region. In this region, the atoms keep some individuality and their interaction can be described with a much higher precision than in the inner region. In fact, for the molecular levels discussed here and for the continuum states as well, the asymptotic part of the potential curve is by far the most important. Usually, the repulsive part of the potential is not known with sufficient high precision to determine the phase accumulated by a wavefunction to a small fraction of π.

To account for experimental data, it is in general necessary to modify the inner part of the potential, to fit the chosen parameters, and to control the way in which this potential is linked to the asymptotic part of the potential. To avoid these delicate tasks, we have chosen an asymptotic method. By this we mean that the Schrödinger equation is solved in the asymptotic region only, as it was done in [18]. The effect of the inner potential is expressed as boundary conditions on the wavefunctions. More precisely we impose to the wavefunctions to vanish at some nodal lines located near the frontier of the asymptotic region [19]. These lines themselves are adjustable parameters which are fitted to the experimental results. In the present case, the data are precise and numerous enough to determine also the main parameters of the asymptotic potential.

The experimental set-up is described in Section 2. The problem of the line assignment is discussed in Section 3. We then describe the asymptotic model that we used for the analysis of the data (Sect. 4). The fitting procedure and the different fits that we performed are presented in Section 5. The results are detailed in Section 6, where we show in particular that neglecting spin-spin and second-order spin-orbit interactions is fully consistent.

[a] e-mail: pierre.pillet@lac.u-psud.fr

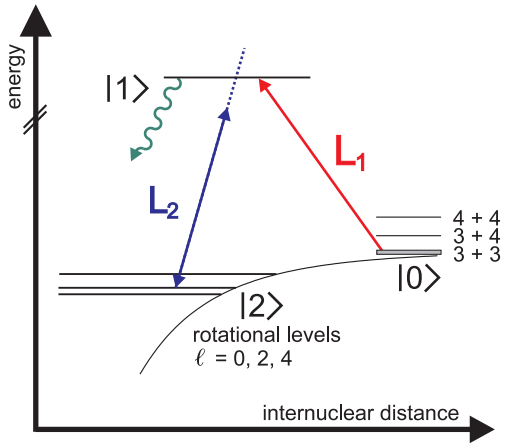

Fig. 1. Coupling scheme for two-photon PA. The two laser fields are denoted L_1 and L_2. The excited molecular state is called $|1\rangle$ and the ro-vibrational level at the ground state asymptote is called $|2\rangle$. The grey shaded area above the lowest hyperfine asymptote (3+3) represents the thermal distribution of the atoms of the MOT in the continuum states $|0\rangle$.

2 Photoassociation scheme

The two-colour photoassociation process and experimental set-up were described in detail in previous articles [17,20,21]. Cesium atoms are loaded out of the back ground gas into a standard magneto-optical trap (MOT). Atoms within the MOT are illuminated with two photoassociation laser fields L_1 and L_2 with frequencies ν_1 and ν_2 respectively. The fields are provided by a Coherent 899 ring titanium-sapphire laser and a DBR diode laser (SDL 5712-H1).

The laser field L_1 couples a continuum state of two colliding cesium atoms, $|0\rangle$, to a single hyperfine and ro-vibrational level $|1\rangle$, selected in the $v' = 1$ vibrational manifold of the electronically singly excited molecular state $(6\,^2S_{1/2} + 6\,^2P_{3/2})\ 1_u$ [21]. The colliding atoms are prepared in a $|0\rangle$ state either by using a dark SPOT or by depumping the MOT before PA into the lower hyperfine state. The PA signal towards the 1_u state is then larger when using atoms populating the higher hyperfine level only. Laser L_2 is frequency tuned to probe resonances between $|1\rangle$ and some ro-vibrational Cs_2 levels $|2\rangle$ near the $(6\,^2S_{1/2} + 6\,^2S_{1/2})$ asymptotes. The coupling scheme is sketched in Figure 1.

Different approaches to determine level energies by two-colour photoassociative spectroscopy were discussed in [17]. As it is shown in this reference, resonant excitation by L_1 of the intermediate level $|1\rangle$ is especially favourable to high precision spectroscopy of molecular levels $|2\rangle$. In the absence of any resonant coupling by L_2, the intermediate level $|1\rangle$ is populated and Cs_2 molecules are formed either in the lowest triplet state $a^3\Sigma_u^+$ or in the molecular ground state $X^1\Sigma_g^+$ by spontaneous emission. These molecules are ionized by resonance enhanced two-photon photoionization and the Cs_2^+ ions are detected with micro channel plates. If a resonance between $|1\rangle$ and $|2\rangle$ is reached by tuning ν_2, a dark resonance is formed between $|0\rangle$, $|1\rangle$, and $|2\rangle$, which avoids the population of $|1\rangle$ and consequently the Cs_2 formation. We have checked that direct population of $|2\rangle$ by a stimulated Raman transition has only a negligible influence on the Cs_2 formation under our experimental conditions. Therefore, the resonance is observed as a dip in the Cs_2^+ ion signal. An overview of a large two-colour photoassociation spectrum is given in Figure 2, and a zoom is reported in Figure 3.

The energy with respect to the lower hyperfine asymptote (3 + 3) of the observed molecular levels is determined by measuring the difference frequency $\Delta\nu = \nu_1 - \nu_2$. In our experiment, this is possible with an uncertainty of ± 3 MHz by comparison of both laser fields in a Fabry-Perot cavity [17]. As it was shown in the latter reference, the measured $\Delta\nu$ are systematically too small in comparison with the actual binding energies, due to the finite energy distribution of atoms in the MOT, which leads in average to a positive collision energy of a few MHz. In consequence, the measured $\Delta\nu$ has to be increased by 3.5 ± 4 MHz.

3 Spectroscopic study

By measuring the positions of levels close to the dissociation thresholds, for which in a classical picture the internuclear distance remains most of the time very large, we investigate in fact the asymptotic region of the lowest electronic states $X^1\Sigma_g^+$ and $a^3\Sigma_u^+$ states of Cs_2. In this region, both states are strongly coupled by the atomic hyperfine interaction, which is very strong in Cs_2 (e.g. [22]). For this reason and because of the small vibrational spacing induced by the high mass of Cs, the spectra in the asymptotic region are expected to be dense and difficult to interpret.

To identify the levels, we use an asymptotic description of the molecular states, that is to say we use two-atom states. The internal quantum numbers of the two atoms, $l_\alpha, s_\alpha, j_\alpha, i_\alpha$ and f_α, are good quantum numbers; $\alpha = 1, 2$ denotes the atom, l_α and s_α are orbital and spin angular momenta, j_α is the fine structure quantum number, i_α is the nuclear spin, and f_α is the total angular momentum of each atom. The quantum numbers f and ℓ, where $\vec{\ell}$ is the angular momentum of the rotation of the nuclei and $\vec{f} = \vec{f}_1 + \vec{f}_2$, are also good quantum numbers, as well as the total angular momentum F and its projection M_F on a space-fixed axis, where $\vec{F} = \vec{f} + \vec{\ell}$. In the absence of external field, the levels are degenerate in M_F. In such a description, a molecular state writes: $|\gamma f \ell F M_F\rangle$, where $\gamma \equiv l_1, s_1, j_1, i_1, f_1, l_2, s_2, j_2, i_2, f_2$. In the whole asymptotic region, that is to say for $R \gtrsim 15a_0$, the quantum numbers f and ℓ remain approximate good quantum numbers. However, it is recalled that, at short internuclear distances, the spin-spin and second order spin-orbit interaction which is especially large in the $a^3\Sigma_u^+$ state [23,24] weakly couples different ℓ and f (but due to the permutation symmetry, one keeps a given parity $p = (-1)^{\ell+\ell_1+\ell_2}$ [25,26]).

In our experiment, the number of accessible hyperfine potentials is strongly limited by the choice of the

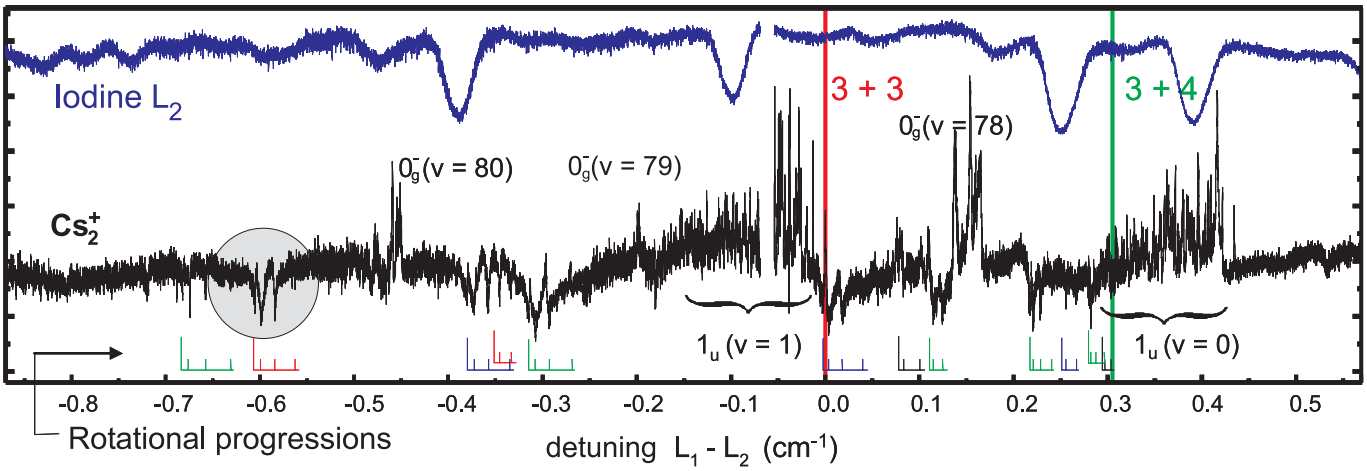

Fig. 2. Overview of the two photon spectrum for $f = 6$ levels. The upper spectrum shows the absorption of the laser L_2 through an iodine cell, which allows us to calibrate very roughly the spectrum. The position of the hyperfine asymptotes $(3 + 3)$ and $(3 + 4)$ are indicated as vertical lines. The assigned rotational progressions are reported below the spectrum. Positive lines correspond to direct PA due to the laser L_2, and the states they correspond to are also depicted. The shaded area emphasizes the rotational series zoomed in Figure 3.

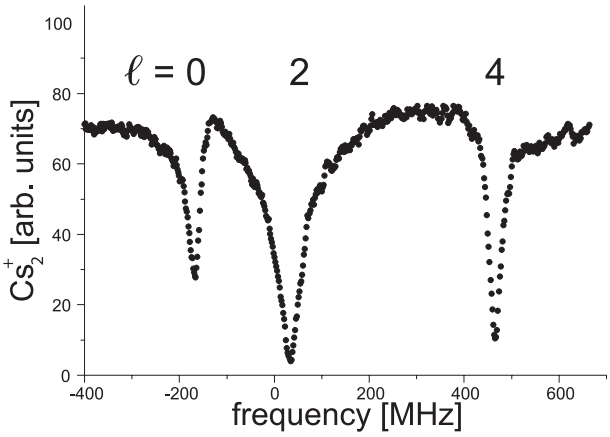

Fig. 3. Rotational series of a vibrational level located at about 0.6 cm^{-1} below the hyperfine asymptote $(3 + 3)$, measured by two-colour PA. The quantum number ℓ characterizes the molecular rotation of the nuclei.

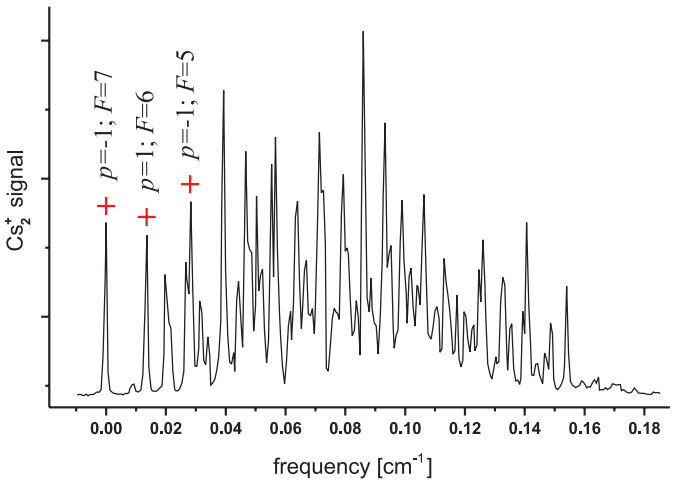

Fig. 4. Detail of the structure of the $v' = 1$ line of the 1_u spectrum, showing the three lines used in the present experiment.

intermediate level $|1\rangle$. Selection rules for the electric dipole coupling between $|1\rangle$ and $|2\rangle$ allows us to avoid overlapping structures and simplifies greatly the interpretation of the recorded spectra. We have chosen the 1_u potential curve for this purpose, because each vibrational level v' offers well separated sub-levels, that have well specified quantum numbers (f', m'_f, F') (m'_f denotes the projection of f' onto the molecular axis). This splitting of the vibrational levels is due to a strong hyperfine and rotational coupling, which was examined in detail previously [21]. We used for the spectroscopic experiments three particular well separated lines of the $v' = 1$ structure of the 1_u PA spectrum, which are shown in Figure 4. The corresponding levels have been shown to correspond to more than 75% to the sets $\{7, 7, 7, -\}$, $\{5, 5, 5, -\}$, or $\{6, 6, 6, +\}$, each set giving the values of f', m'_f, F' and the sign of the parity p [27].

The levels of the ground state potentials that can be observed in our experiment are those which are coupled by the light of the laser L_2 to these three particular 1_u levels. Selection rules impose first that the parity of the ℓ value is conserved. This explains the appearance of even ℓ only in Figure 3, since in this case, the state $|1\rangle$ corresponds to the set $\{7, 7, 7, -\}$, that is to even ℓ values. The selection rules also impose that $F' - F = 0, \pm 1$ and $f' - f = 0, \pm 1$. One can show that some electronic states, namely those with $f = 8, 7, 5, 3, 1$ and even ℓ and those with $f = 6, 4, 2$ and odd ℓ correlate only to the $a^3\Sigma_u^+$ state (see Fig. 6). Thus, *ungerade* symmetry is kept at any internuclear distance. Consequently, dipole coupling of these states to the 1_u is thus forbidden. Furthermore, we have calculated the dipole coupling between the main component of the decomposition of the 1_u states in a $|\gamma' f'_1 f'_2 f' m'_f F' M'\rangle$ state basis (in the three cases, the main component represents

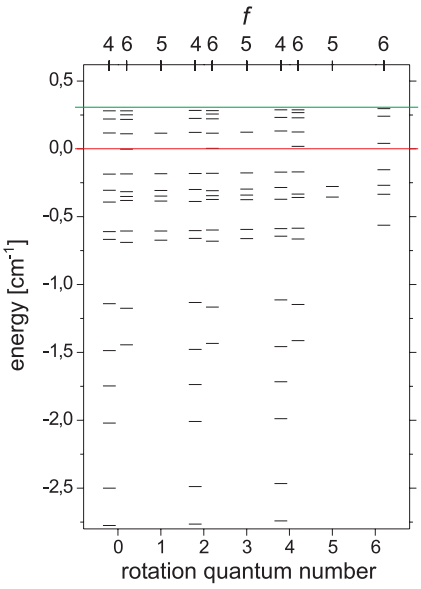

Fig. 5. Overview of measured levels and their assignment. The rotation quantum number ℓ characterizes the rotation of the nuclei. The zero energy is taken at the lowest asymptote $(3+3)$.

more than 40% of the decomposition). For the observed ℓ values, the coupling strongly favours the quantum numbers $f = 4$, $F = 4$ (resp. $f = 5$, $F = 5$ and $f = 6$, $F = 6$) when starting from the $\{5, 5, 5, -\}$ 1_u level (resp. $\{6, 6, 6, +\}$ and $\{7, 7, 7, -\}$).

More than 100 asymptotic levels of the coupled electronic states $X^1\Sigma_g^+$ and $a^3\Sigma_u^+$ were identified and measured in a 3.5 cm^{-1} energy interval below the highest hyperfine asymptote $(4+4)$. Rotational angular momenta ℓ up to 6 were observed. An overview of the data is given in Figure 5. Levels with positive energies are located above the lowest hyperfine asymptote and are subject to predissociation due to coupling to energetically lower hyperfine channels. The level energies are listed in the appendix.

The uncertainty of the level energy with respect to the lowest hyperfine asymptote is ±12 MHz for the $f = 6$ levels and ±24 MHz for the others. It includes possible errors from the frequency measurement, the uncertainty of the determined line shift due to the thermal distribution of atoms in the MOT and errors from the determination of the line position, which is limited by the noise of the Cs_2^+ signal [17]. The f-dependence of the uncertainty simply accounts for slightly different experimental conditions and signal-to-noise ratios.

4 Multichannel asymptotic model

The asymptotic Hamiltonian writes:

$$H^{\text{asympt}}(R) = -\frac{\hbar^2}{2\mu R}\frac{\partial^2}{\partial R^2}R + \frac{\vec{\ell}^2}{2\mu R^2} + H^{\text{elec}}(R) \quad (1)$$

where $H^{\text{elec}}(R)$ contains the atomic hyperfine structure, the electrostatic interaction and the exchange interaction. Multipole expansion of electrostatic interaction is used, including so-called damping coefficients $f_n(R)$ [28]:

$$\sum_{n=6,8,10,12} f_n(R) C_n / R^n \quad (2)$$

where the damping coefficients are given by

$$f_n(R) = \left[1 - e^{-a(R-nb)}\right]^n \quad (3)$$

and the asymptotic exchange interaction [29], expressed in the Hund's case (a), writes

$$(-1+2S) D R^\gamma e^{-2\alpha R} \quad (4)$$

where S denotes the molecular spin, and where α is related to the ionization energy by $\alpha = \sqrt{2E_{\text{ion}}}$. The spin-spin and second-order spin-orbit interactions are not included (see discussion later). This Hamiltonian mixes the states $|\gamma f \ell F M_F\rangle$ with different γ and the energies are degenerate in F and M_F. Any wavefunction can be written in a fragmentation channel basis [21,26]:

$$\Psi_{f\ell}^{\text{total}}(\vec{R}) = \sum_\gamma \Psi_{\gamma f\ell}(\vec{R}) G_{\gamma f\ell}(R)/R. \quad (5)$$

The Schrödinger equation leads then to a system of coupled equations for the radial components $G_{\gamma f\ell}(R)$ of the multichannel wave function, that we solve in the asymptotic region only, that is for $R > R_0$, where R_0 is of the order of $15a_0$. This is not only the region where the above form of the Hamiltonian is valid but also the region where the hyperfine coupling is active. In equation (5), the electronic states $\Psi_{\gamma f\ell}(\vec{R})$ must form a basis set which can be, for instance, a set of $|\gamma f \ell F M_F\rangle$ states ("uncoupled" basis), but it could also be the set of adiabatic potential states resulting from the diagonalization of H^{elec} ("adiabatic" basis). In the former case, the system of radial coupled equations have a very straightforward matrix form, whereas in the latter case one has to include the so-called "kinetic coupling" terms, which require the knowledge at any R of the eigenvectors of H^{elec}.

The principle of our theoretical treatment is to express the effect of potentials below R_0 as boundary conditions on the radial wave functions. The inner part of the molecular potentials yields near R_0 an accumulated phase [13] to the vibrational wavefunctions, or, in other words, it determines the positions of the nodes of these wave functions. Since the levels we study are weakly bound, experimental energies lie in a very narrow range (3.5 cm^{-1}) compared to the depth of the two potentials of the ground state (about 250 cm^{-1} and 3500 cm^{-1} for the $X^1\Sigma_g^+$ and $a^3\Sigma_u^+$ potentials, respectively). Then the positions of the nodes of the radial wavefunctions are expected to depend linearly on the level energy [19], so that one will use nodal *straight* lines (see Fig. 7).

In the case of a single channel problem, the wavefunction has only one radial component and one has to consider one nodal line only. The variation with ℓ of the node positions is easily shown to be proportional to $\ell(\ell+1)$, for instance by using a WKB formula including a centrifugal energy potential. The nodal line can thus be described by:

$$R_\ell(E) = R^0 + \mathcal{A}E + \mathcal{B}\ell(\ell+1). \quad (6)$$

The fact that $\mathcal{B}$ does not depend on ℓ also appears in the WKB treatment.

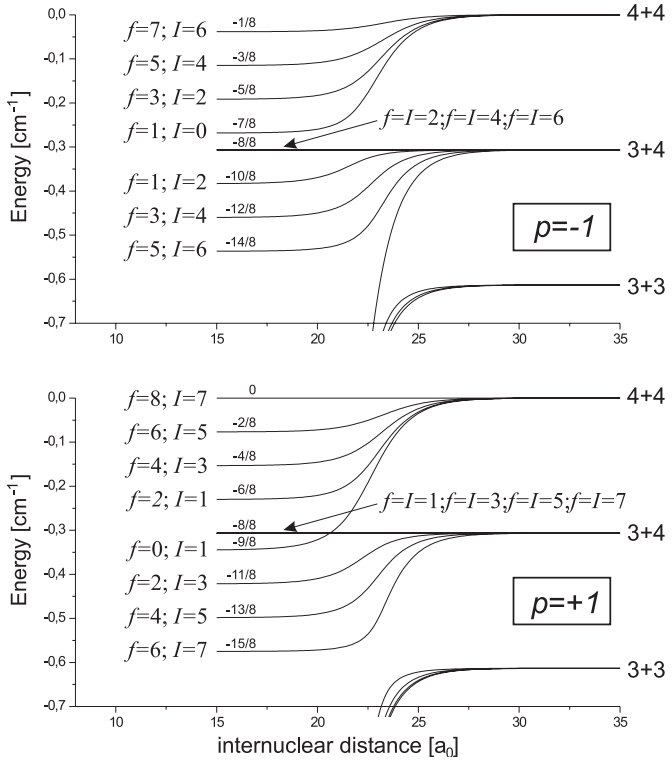

Fig. 6. Detail of the potential curves in the asymptotic region. The highest potential curve ($f = 8,\ I = 7$) has been subtracted to all ones. To each curve is associated the fraction of the atomic hyperfine splitting which characterizes its relative position in the inner region (see text).

In the multichannel case, the situation is more complex. As already mentioned, at very long internuclear distances, the good quantum numbers are f_1, f_2, f, F and M_F and the energies are degenerate in F and M_F. Still in the asymptotic region, but at shorter distances, the atomic hyperfine coupling becomes small compared to the exchange interaction. Around $R_0 \simeq 15a_0$, the *gerade/ungerade* character becomes almost well defined and the electronic spin S and the nuclear spin I become good quantum numbers (see Fig. 6). Thus around R_0, boundary conditions are settled on nodal straight lines described by:

$$R_{ISf\ell}(E) = R^0_{ISf} + \mathcal{A}_{ISf}E + \mathcal{B}_{ISf}\ell(\ell+1). \qquad (7)$$

The coupled radial equations are solved using the following boundary conditions:

(i) on the chosen nodal lines, radial components of the wavefunctions written in the adiabatic basis have to vanish;
(ii) as R goes to infinity, bound level wavefunctions have to vanish and the wavefunctions of resonances lying above the lowest dissociation limit have to be purely outgoing waves, according to the formalism of Siegert states [30]. Bound levels and resonances are treated in the same way using complex energy calculations.

The numerical integration is performed starting from large R values and in the uncoupled basis $|\gamma f \ell F M_F\rangle$. A set of linearly independent solutions fulfilling conditions (ii) is calculated and the level energies or the resonance positions and widths are obtained from cancellation of the determinant of the matrix expressing conditions (i). Calculating in this way theoretical energy values and comparing them to the measured values in a least square fit with the measured energies for levels and resonances leads to simultaneous determination of the nodal lines and of selected molecular parameters of the asymptotic potentials.

5 Statistical treatment

The fitting procedure consists in a non-linear least square fit, minimizing the reduced chi-square,

$$\chi^2_{\rm red} = \frac{1}{N-k}\sum_{i=1,N}\frac{\left(E_i^{\rm exp} - E_i^{\rm cal}\right)^2}{\sigma_i^2} \qquad (8)$$

where $E_i^{\rm exp}$ and $E_i^{\rm cal}$ are N observed and calculated energies and σ_i denotes the experimental uncertainty in the determination of $E_i^{\rm exp}$, k being the number of parameters. As mentioned above, we provide to the fitting procedure three parameters for each nodal line: an origin R^0, a slope $\mathcal{A}$, and the rotation dependence of the origin given by $\mathcal{B}$. Consequently, in order to describe the nodal lines associated with the $\{f = 4, +\}$, $\{f = 5, -\}$ and $\{f = 6, +\}$ manifolds that we measured, we provide to the fitting procedure 9 parameters associated with the nodal lines of each manifold. We also consider as adjustable some parameters related to the asymptotic potential: the dispersion coefficients, C_6, C_8, C_{10}, and the amplitude D of the exchange interaction. Thus the fit involves in principle 31 parameters to fit 103 experimental energies.

In view of such a high number of parameters, stochastic fitting procedure appears to be more relevant than deterministic fitting procedures, such as gradient or simplex procedures. It has been implemented using self-adaptative evolution strategies [31], which are known to be the most efficient among evolutionary algorithms [32]. One run after the other, this stochastic algorithm provides parameter sets which lie in a wide range of quite reasonable parameters. These sets are then given as initial guess to a deterministic minimum seeking. Finally, in order to determine uncertainties on the parameters determination, we computed the complete covariance matrix, derived from the Hessian matrix calculated at the best fit point.

First attempts have shown that the number of parameters needs to be reduced to achieve convergence. As all singlet potential curves are degenerate in the inner region, we use the same nodal line for all sets with $S = 0$, reducing the number of parameters to 25. It also appears that the 16 experimental energies labeled by $f = 5$ do not fix correctly the 6 corresponding nodal line parameters: suppressing these data together with these parameters leads to 19 parameters and 87 level energies. Figure 6 shows that near $15a_0$, the adiabatic triplet potential curves are parallel and obey a very regular arrangement, their energy differences $\Delta V(I, f)$ being simply multiples of the eighth

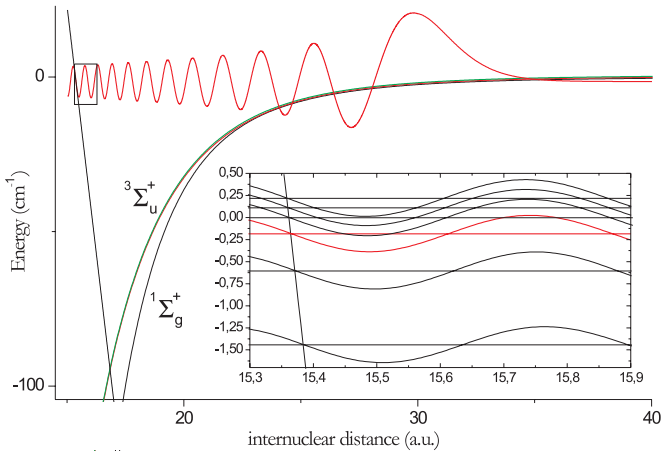

Fig. 7. Asymptotic part of one component (a triplet one, that is with *ungerade* character at short distance) of a typical multichannel wave function written in the adiabatic basis. Inner boundary conditions are settled near $15a_0$. The inset shows the alignment, on the corresponding nodal line, of the nodes of several such wavefunctions close to the $(3+3)$ asymptote.

of the atomic hyperfine splitting, which can be found in Figure 6. Assuming that molecular hyperfine structure remains correctly described by the atomic Hamiltonian up to the triplet inner potential wall, the adiabatic triplet curves are parallel for $R < R_0$. The relative positions of the adiabatic triplet curves imply very simple relationships between the different triplet nodal lines. First, they have the same slope $\mathcal{A}_1$ and the same ℓ-dependence $\mathcal{B}_1$. Moreover, the values R^0_{ISf} at the origin obey the following law:

$$R^0_{ISf} = R^0_{I=7\,S=1\,f=8} - \mathcal{A}_1 \Delta V(I,f). \qquad (9)$$

The number of parameters is then reduced to 10. This reduction has been also justified from a purely statistical point of view, using local linear multiple regression, that we do not detail here.

Even though, the convergence of the algorithm remains laborious and it appears that it is probably impossible to safely determine simultaneously the four chosen parameters of the asymptotic potential. It is clear that our data, which concern levels close to the asymptote, with outer Condon points of the order of $25-50a_0$, yield more information on the C_6 coefficient than on the others. Thus, we do a first fit by keeping only C_6 as adjustable parameter and by fixing C_8, C_{10} and D. For C_8 and C_{10} we used the values $C_8 = 9.630 \times 10^5$ a.u. and $C_{10} = 1.35912 \times 10^8$ a.u. obtained by Amiot and Dulieu [33], which performed the most precise determination (2% uncertainty) of these parameters. To be fully consistent, we choose the same parameters as these authors. We introduced the same damping coefficients and we used the same theoretical asymptotic exchange term, with (in atomic units) $D = 0.00110$, $\alpha = 0.535$ and $\gamma = 5.542$ [29]. A rapid convergence of the algorithm leads then to a reduced chisquare value of $\chi^2_{\rm red} = 0.777$ (Tab. 2, fit 1). We checked the local linearity of calculated energies with respect to the parameters, and under that conditions, uncertainties on the values of the adjustable parameters are obtained from the second derivative matrix, the so-called Hessian matrix, in 7 dimensions and from the associated covariance matrix. The obtained value of C_6 is 6840.8 a.u., with a standard uncertainty of 13.6 a.u. which accounts for correlations between all parameters [34,35].

Table 1. *Estimated* uncertainties one would obtain on some adjusted parameters if fixing the others, denoted by an $\times$ symbol. The whole set of nodal lines is described by six parameters. The results of Amiot and Dulieu are recalled for comparison.

model	C_6	C_8	C_{10}	D
asymptotic model	2%	48%	61%	40%
	1.2%	13%	46%	$\times$
	0.20%	$\times$	$\times$	$\times$
	0.25%	$\times$	$\times$	9.7%
reference [33]	1.5%	2%	2%	$\times$

It is also possible to obtain an *estimation* of the uncertainties one would obtain on other parameters by calculating the Hessian matrix in the n-dimensional space (with $n > 7$) including these parameters. The results are summarized in Table 1. As the uncertainties on C_8 and C_{10} are much larger than those of reference [33], we will keep the values of these two parameters as fixed. The optimized C_6 value obviously depends on these fixed values. This dependence remains however linear in a large range and this justifies our statistical treatment of uncertainties. With the obtained numerical values, this dependence writes:

$$\Delta C_6 = 310\Delta C_8/C_8 + 133\Delta C_{10}/C_{10} + 53.3\Delta D/D \quad (10)$$

where ΔC_8 (resp. ΔC_{10}, ΔD) stands for a variation of C_8 (resp. C_{10}, D) from the value reported in Table 2 (fit 1). Equation (10) can also be used to deduce the uncertainty on C_6 which comes from the uncertainty of the fixed parameters. Adding quadratically the independent uncertainties, we find an uncertainty on the C_6 value of 15.2 a.u.

At this point of the study, it is possible to re-introduce the $f = 5$ data that we leaved previously. Thanks to the introduction of the relationship between the triplet nodal lines, no additional parameter is then required. A new fit (Tab. 2, fit 2), with 7 parameters and 103 level energies, gives $\chi^2_{\rm red} = 0.727$, with a C_6 value of (6841.77 ± 12.93) a.u., and with a dependence on the fixed parameters almost identical to the previous one. Taking into account the 2% error on the C_8 and C_{10} values, we obtain (6841.8 ± 14.5) a.u.

The asymptotic exchange interaction plays an important role in the calculation, as it fixes the mixing of the different channels which is far from negligible. It seems therefore possible to determine the parameter D of equation (4), as suggested by Table 1. A final fit with 103 level energies and 8 parameters (Tab. 2, fit 3) gives $\chi^2_{\rm red} = 0.726$, with $C_6 = (6846.2 \pm 13.7)$ a.u. and $D = 0.001187 \pm 0.000086$ a.u. The final uncertainty on C_6, including C_8 and C_{10} errors, is 15.6 a.u., whereas the the final uncertainty on D is 0.000088 a.u.

Table 2. Different fits discussed in Section 5. Reduced χ^2 values are given, which account for the number of adjusted parameters (see text). Fixed values are between brackets. All uncertainties are one-parameter standard uncertainties. Therefore, they do not include the uncertainty induced by the fixed parameters: only the final uncertainty $\sigma_{C_6}^{\text{final}}$ accounts for the uncertainties on C_8 and C_{10} given in reference [33]. Every fixed value is taken from reference [33]. $R^0_{I=5,S=1,f=4}$ has been used in the fits instead of $R^0_{I=7,S=1,f=8}$ like in equation (9). The correspondence is straightforward, just by changing the reference potential in the equation defining the nodal lines.

	fit 1	fit 2	fit 3
levels	87	103	103
parameters	7	7	8
χ^2_{red}	0.777	0.727	0.726
coefficients			
C_6 (a.u.)	6840.76 ± 13.65	6841.77 ± 12.93	6846.17 ± 13.70
$C_8(10^5$ a.u.)	[9.630]	[9.630]	[9.630]
$C_{10}(10^8$ a.u.)	[1.35912]	[1.35912]	[1.35912]
$C_{12}(10^{10}$ a.u.)	[2.901]	[2.901]	[2.901]
$D(10^{-3}$ a.u.)	[1.10]	[1.10]	1.18722 ± 0.08633
nodal lines			
$R^0_{S=0}$	15.075539	15.075853	15.095202
(a_0)	± 0.003503	± 0.003316	± 0.019267
$\mathcal{A}_{S=0}$	-7.5867	-7.5350	-7.5819
$(10^{-3} a_0/\text{cm}^{-1})$	± 0.1902	± 0.1801	± 0.1834
$\mathcal{B}_{S=0}$	5.4281	5.2977	5.3113
$(10^{-5} a_0)$	± 0.5475	± 0.5135	± 0.5124
$R^0_{I=5,S=1,f=4}$	15.291023	15.291382	15.263980
(a_0)	± 0.005284	± 0.005009	± 0.027961
$\mathcal{A}_{S=1}$	-17.8135	-17.8205	-17.6710
$(10^{-3} a_0/\text{cm}^{-1})$	± 0.1866	± 0.1785	± 0.2355
$\mathcal{B}_{S=1}$	10.3267	10.3515	10.3948
$(10^{-5} a_0)$	± 0.4869	± 0.4608	± 0.4690
$\sigma_{C_6}^{\text{final}}$ (a.u.)	15.2	14.5	15.6

6 Discussion of the results

The reduced chi-square values of the three fits of Table 2 are all smaller than one. This might indicate that the experimental uncertainties on energy values have been overestimated, but it also reflects the quality of the model and of the fit [34]. This low chi-square value is also taken into account in the parameters uncertainties. Namely, we use a standard procedure which amounts to a global scaling of experimental uncertainties such that the chi-square value would be one. The three C_6 values are fully compatible. It is worthwhile noticing that the introduction of the data corresponding to the $\{f = 5\}$ manifold (Tab. 2, fit 2) did not either increase the reduced chi-square nor affect the C_6 value: this is a strong indication of the prediction ability of the model. One could calculate level energies corresponding to all $\{f, p\}$ manifolds. Scattering lengths can also be calculated. For instance, we have calculated the scattering length associated with the the lowest asymptote of the $\{f = 6, +\}$ manifold which is usually denoted by $a_{3,3}$, which corresponds to zero-energy collisions between atoms polarized in the lowest hyperfine state $f_\alpha = 3$, with the maximum space-fixed projection $M_{f_\alpha} = \pm 3$. Using our data, the calculation of this scattering length leads to uncertainties so large that they make this determination irrelevant. Nevertheless, such large error bars on the scattering length value should be very efficiently shrunken by introducing in our study some collision data, more sensitive to the scattering length.

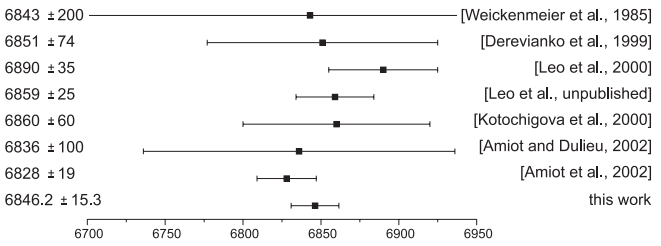

Fig. 8. Comparison of the values and uncertainties of the different determinations of the C_6 van der Waals coefficient of cesium. The only ab initio value is the one of Derevianko et al.

The uncertainty we obtain on the final value of the C_6 coefficient is the smallest among the numerous determinations presently available (see Fig. 8). The van der Waals C_6 coefficient of cesium has indeed been the object of numerous studies, theoretical and experimental as well, especially because of the numerous difficulties encountered before the achievement of Bose-Einstein condensation of cesium atoms [36]. The value that we obtain

is in very good agreement with the most recent ones (see Fig. 8). On the contrary, our value is not compatible with the 6510±70 a.u. value we determined in [37] from the analysis of the line intensity modulations in a PA spectrum. Several possible explanations of that discrepancy are presently studied.

It is important to mention that our determination relies essentially on experimental data. Excited molecular states do not play any role in the analysis and we do not use any ab initio potential, since reference [33] provides a Rydberg-Klein-Rees (RKR) potential. We remind that the adjusted C_6 value depends on the chosen values of the other parameters of the asymptotic potential, but the dependence is linear in a large domain and can be calculated.

We have also obtained the first determination of the exchange interaction term from experimental data. The value is in good agreement with the ab initio value of reference [29], 0.00110, for which no uncertainty was given, and about twice smaller than the one of reference [38], which found $D = 0.00243$ using the same values for α and γ as we use.

Within our experimental precision, the asymptotic model we developed here is fully justified. We recall here the assumptions that have been made. Firstly, and this assumption is supported by the model, we assume that, near the frontier between inner and asymptotic regions R_0, the nodes of the radial multichannel wavefunctions, written in the adiabatic basis, are straight lines. Secondly we also made weaker assumptions, which could eventually be avoided depending on the considered data set and on the experimental precision. We use several a priori relations between the different nodal lines involved in the analysis: their value at the origin depends linearly in $\ell(\ell+1)$, the nodal lines are the same for all singlet curves and the triplet nodal lines are all parallel, their relative positions depend in a simple manner on the relative positions of the triplet potential curves near R_0. Let us also mention that we consider the usual model for the asymptotic potential, with damped C_n ($n = 6, 8, 10, 12$) dispersion coefficients and asymptotic exchange term and that we neglect in our asymptotic Hamiltonian spin-spin and retardation effects. The latter two effects are indeed completely negligible at the interatomic distances relevant for the concerned bound states and they are also completely negligible as compared with the collision energies corresponding to the concerned quasi-bound states.

Limitations of our asymptotic model could in fact essentially arise from interactions which, in the asymptotic point of view, are *hidden* in the inner region of the potential curves, such as the spin-spin and second-order spin-orbit interactions. These interactions are known to be sometimes very important in the cesium case, for instance in collisions between ultracold cesium atoms [23]. These interactions couple different f and ℓ values and can be responsible for very high inelastic collision rates [39,40]. In our treatment these interactions are somehow taken into account in the determination of the nodal lines by a fit on experimental data. However, they could in principle prevent the nodal lines from being straight lines, in the case of zeroth-order quasi-coincidence of interacting states. They could destroy the $\ell(\ell+1)$-dependence of the origin of the nodal lines and they could distord the simple relation between the triplet lines. Careful examination of the residuals given by the fits does not indicate any of these disturbing effects. In fact a single channel calculation shows that for a typical bound state, the radial wavefunction is located at rather large distance ($\sim 50 a_0$), so that the perturbation matrix element associated with these interactions is below 10^{-5} cm^{-1}. This is more than one order of magnitude smaller than our experimental resolution, and neglecting these terms does not perturb neither the level energies nor the associated wavefunctions, which confirms our analysis.

7 Conclusion

We have measured and assigned 103 energies of high lying levels and near-threshold resonances of the ground state of Cs_2. These energies have been interpreted with the help of only eight adjustable parameters. Six of them characterize the nodal lines, which account for the inner part of the potentials, which is not introduced in the calculations. The other two parameters, the van der Waals C_6 coefficient and the amplitude of the asymptotic exchange interaction, characterize the asymptotic potential, together with C_8, C_{10}, C_{12}, which were fixed parameters in the fit. From the asymptotic potential and the nodal lines provided by the analysis, one can in principle predict a lot of other quantities such as near threshold levels and resonances with different f and ℓ values, or scattering lengths. The good accuracy of the predictions has already been tested by introducing in the fit a new set of data ($f = 5$).

The two-colour photoassociation scheme that we used should allow further spectroscopic studies of ground state potentials. In particular it should be possible to complement the $X^1\Sigma_g^+$ spectrum obtained by molecular spectroscopy [33]. The asymptotic model will allow us to predict the energy ranges to be investigated. For higher resolution in the spectroscopy of the ground state potentials, it would be interesting to use a Bose-Einstein condensate, in which the width of the two-photon photoassociation lines can be as low as one kiloHertz [41]. Frequency calibration and energy measurements would certainly become more difficult, frequency collisional shifts would have to be taken into account, but increasing the experimental precision would increase the precision on the determination of the parameters. Multiplets corresponding to different F values could be resolved, allowing direct observation of the influence of the second-order spin-orbit interaction on level energies.

The results presented here illustrate very well the efficiency of two-colour photoassociation spectroscopy associated with an asymptotic model for the description of near threshold bound and quasi-bound levels of the ground state potentials of cesium. We obtained the first experimental determination of the asymptotic exchange amplitude, and a very accurate value of the van der Waals coefficient.

Table 3. Experimental level energies with respect to the asymptote $(f_1 = 3) + (f_2 = 3)$, measured by two-photon photoassociation, reported in cm^{-1}. All energies take into account the systematic shift due to the thermal distribution of the atoms in the MOT. Experimental uncertainties have been estimated to be 0.0008 cm^{-1} (24 MHz) for $f = 4$ and $f = 5$ levels and 0.0004 cm^{-1} (12 MHz) for $f = 6$ levels, due to different experimental conditions. Below each experimental energy is reported in italics the corresponding residual (observed minus calculated energy difference), calculated from the fit 3 of Table 2.

f	p	ℓ	energy *residual*	f	p	ℓ	energy *residual*	f	p	ℓ	energy *residual*	f	p	ℓ	energy *residual*
4	+1	4	0.288135	4	+1	0	−1.140299	5	−1	3	−0.374119	6	+1	2	−0.179912
			−0.000312				*−0.000194*				*0.000279*				*0.000225*
4	+1	2	0.282818	4	+1	4	−1.456668	5	−1	1	−0.384425	6	+1	0	−0.184366
			−0.000418				*0.000226*				*0.001073*				*−0.000004*
4	+1	0	0.280479	4	+1	2	−1.476865	5	−1	3	−0.594053	6	+1	6	−0.268944
			−0.000486				*0.000387*				*0.000164*				*0.000153*
4	+1	4	0.231489	4	+1	0	−1.486747	5	−1	1	−0.605528	6	+1	2	−0.307504
			−0.000708				*−0.000749*				*−0.000901*				*0.000314*
4	+1	2	0.223746	4	+1	4	−1.715414	5	−1	3	−0.661207	6	+1	0	−0.314706
			−0.000464				*0.000224*				*0.000734*				*−0.000436*
4	+1	0	0.220762	4	+1	2	−1.736247	5	−1	1	−0.673216	6	+1	4	−0.332876
			0.000558				*0.000624*				*0.000718*				*−0.000323*
4	+1	4	0.131475	4	+1	0	−1.746400	6	+1	6	0.296305	6	+1	2	−0.345457
			0.000010				*−0.000421*				*−0.000257*				*0.000017*
4	+1	2	0.121978	4	+1	4	−1.987344	6	+1	4	0.287746	6	+1	0	−0.351271
			0.000419				*0.000764*				*0.000206*				*−0.000289*
4	+1	0	0.117662	4	+1	2	−2.008622	6	+1	2	0.282137	6	+1	6	−0.334478
			0.000364				*0.000948*				*0.000095*				*−0.000487*
4	+1	4	−0.170641	4	+1	0	−2.019942	6	+1	0	0.279646	6	+1	4	−0.357685
			0.001183				*−0.001163*				*−0.000381*				*−0.000196*
4	+1	2	−0.181867	4	+1	4	−2.465681	6	+1	4	0.267385	6	+1	2	−0.372691
			−0.000184				*−0.000348*				*0.0000166*				*0.000133*
4	+1	0	−0.186192	4	+1	2	−2.488703	6	+1	2	0.256153	6	+1	0	−0.379727
			−0.000277				*0.000536*				*0.000248*				*−0.000256*
4	+1	4	−0.283949	4	+1	0	−2.499954	6	+1	0	0.251314	6	+1	6	−0.562633
			−0.000408				*−0.001152*				*0.000312*				*−0.000965*
4	+1	2	−0.298744	4	+1	4	−2.741280	6	+1	6	0.241256	6	+1	4	−0.584139
			−0.000488				*−0.000094*				*0.000248*				*−0.000263*
4	+1	0	−0.305567	4	+1	2	−2.764730	6	+1	4	0.228914	6	+1	2	−0.598491
			−0.001017				*−0.000003*				*−0.000072*				*0.000439*
4	+1	4	−0.371978	4	+1	0	−2.774407	6	+1	2	0.221035	6	+1	0	−0.605053
			−0.000232				*0.000417*				*−0.000111*				*0.000117*
4	+1	2	−0.386977	5	−1	3	0.122666	6	+1	0	0.217515	6	+1	4	−0.664004
			−0.000220				*−0.000258*				*−0.000221*				*−0.000061*
4	+1	0	−0.392467	5	−1	1	0.116123	6	+1	4	0.124940	6	+1	2	−0.680546
			−0.001477				*0.000315*				*−0.000170*				*0.000211*
4	+1	4	−0.587732	5	−1	3	−0.176746	6	+1	2	0.115245	6	+1	0	−0.688730
			−0.000072				*−0.000001*				*0.000077*				*−0.000741*
4	+1	2	−0.602127	5	−1	1	−0.183700	6	+1	0	0.110777	6	+1	4	−1.146618
			0.000122				*0.000078*				*−0.000113*				*0.000091*
4	+1	0	−0.609009	5	−1	5	−0.276856	6	+1	6	0.040116	6	+1	2	−1.165335
			−0.000498				*0.000008*				*−0.000312*				*0.000352*
4	+1	4	−0.643434	5	−1	3	−0.295764	6	+1	4	0.018298	6	+1	0	−1.174056
			−0.000622				*0.000183*				*0.000158*				*−0.000225*
4	+1	2	−0.659975	5	−1	1	−0.306419	6	+1	2	0.004433	6	+1	4	−1.413306
			−0.000431				*0.000144*				*0.000548*				*0.000271*
4	+1	0	−0.667342	5	−1	3	−0.339781	6	+1	0	−0.002237	6	+1	2	−1.433054
			−0.000604				*−0.000755*				*−0.000346*				*0.000806*
4	+1	4	−1.113209	5	−1	1	−0.347402	6	+1	6	−0.153935	6	+1	0	−1.443212
			−0.000281				*0.000920*				*0.001119*				*−0.000643*
4	+1	2	−1.131525	5	−1	5	−0.354826	6	+1	4	−0.170398				
			0.000420				*−0.000044*				*−0.000062*				

The authors thank O. Dulieu and C. Amiot for many helpful discussions, as well as B. Laburthe-Tolra. This work was supported by "Action Contertée Incitative Photonique" of the French research Ministry, and by the "Cold Molecules Network", contract no. HPPRN-CT-2002-00290. This work was also supported by a fellowship for Ch. Lisdat within the "Postdoc-Programme" of the German Academic Exchange Service (DAAD).

Appendix

Table 2 gives in details the best fit parameters obtained in the different fits presented in Section 5. Standard uncertainties are also given for all the adjusted parameters.

Table 3 reports all the experimental level energies included in the fit, with respect to the asymptote $(3 + 3)$. All energies take into account the systematic shift of

3.5 MHz due to the thermal distribution of Cs atoms in the MOT [17], as mentioned in Section 2.

References

1. J. Weiner, V.S. Bagnato, S.C. Zilio, P.S. Julienne, Rev. Mod. Phys. **71**, 1 (1999)
2. W.C. Stwalley, H. Wang, J. Mol. Spectrosc. **195**, 194 (1999)
3. F. Masnou-Seeuws, P. Pillet, Adv. At. Mol. Opt. Phys. **47**, 53 (2001)
4. P.D. Lett, K. Helmerson, W.D. Philips, L.P. Ratliff, S.L. Rolston, M.E. Wagshul, Phys. Rev. Lett. **71**, 2200 (1993)
5. W.C. Stwalley, Y.-H. Uang, G. Pichler, Phys. Rev. Lett. **41**, 1164 (1978)
6. E. Tiemann, H. Knöckel, H. Richling, Z. Phys. D **37**, 323 (1996)
7. M. Elbs, O. Keck, H. Knöckel, E. Tiemann, Z. Phys. D **42**, 49 (1997)
8. A. Fioretti, D. Comparat, A. Crubellier, O. Dulieu, F. Masnou-Seeuws, P. Pillet, Phys. Rev. Lett. **80**, 4402 (1998)
9. C.J. Williams, E. Tiesinga, P.S. Julienne, H. Wang, W.C. Stwalley, P.L. Gould, Phys. Rev. A **60**, 4427 (1999)
10. A. Fioretti, D. Comparat, C. Drag, C. Amiot, O. Dulieu, F. Masnou-Seeuws, P. Pillet, Eur. Phys. J. D **5**, 389 (1999)
11. A.N. Nikolov, J.R. Enscher, E.E. Eyler, H. Wang, W.C. Stwalley, P.L. Gould, Phys. Rev. Lett. **84**, 246 (2000)
12. E.R.I. Abraham, W.I. McAlexander, C.A. Sackett, R.G. Hulet, Phys. Rev. Lett. **74**, 1315 (1995)
13. C.C. Tsai, R.S. Freeland, J.M. Vogels, H.M.J.M. Boesten, J.R. Gardner, D.J. Heinzen, B.J. Verhaar, Phys. Rev. Lett. **79**, 1245 (1997)
14. B. Laburthe Tolra, C. Drag, P. Pillet, Phys. Rev. A **64**, 61401(R) (2001)
15. J.L. Bohn, P.S. Julienne, Phys. Rev. A **54**, R4637 (1996)
16. J.L. Bohn, P.S. Julienne, Phys. Rev. A **60**, 414 (1999)
17. Ch. Lisdat, N. Vanhaecke, D. Comparat, P. Pillet, Eur. Phys. J. D **21**, 299 (2002)
18. J.M. Vogels, R.S. Freeland, C.C. Tsai, B.J. Verhaar, D.J. Heinzen, Phys. Rev. A **61**, 043407 (2000)
19. A. Crubellier, O. Dulieu, F. Masnou-Seeuws, H. Knöckel, M. Elbs, E. Tiemann, Eur. Phys. J. D **6**, 211 (1999)
20. D. Comparat, C. Drag, A. Fioretti, O. Dulieu, P. Pillet, J. Mol. Spectrosc. **195**, 229 (1999)
21. D. Comparat, C. Drag, B. Laburthe Tolra, A. Fioretti, P. Pillet, A. Crubellier, O. Dulieu, F. Masnou-Seeuws, Eur. Phys. J. D **11**, 59 (2000)
22. H. Weckenmeier, U. Diemer, W. Demtröder, M. Broyer, Chem. Phys. Lett. **124**, 470 (1986)
23. F.H. Mies, C.J. Williams, P.S. Julienne, M. Krauss, J. Res. Inst. Stand. Technol. **101**, 521 (1996)
24. S. Kotochigova, E. Tiesinga, P.S. Julienne, Phys. Rev. A **63**, 012517 (2000)
25. E. Tiesinga, C.J. Williams, P.S. Julienne, K.M. Jones, P.D. Lett, W.D. Phillips, J. Res. Inst. Stand. Technol. **101**, 505 (1996)
26. Bo Gao, Phys. Rev. A **54**, 2022 (1996)
27. B. T'Jampens, Ph. D. thesis, Université de Paris-Sud — Orsay, Paris XI (2002)
28. W. Weickenmeier, U. Diemer, M. Wahl, M. Raab, W. Demtröder, J. Chem. Phys. **82**, 5354 (1985)
29. G. Hadinger, G. Hadinger, S. Magnier, M. Aubert-Frecon, J. Mol. Spectrosc. **175**, 441 (1996)
30. A.J.F. Siegert, Phys. Rev. **56**, 750 (1939)
31. C++ sources available on `http://eodev.sourceforge.net/`
32. Hans-Paul Schwefel, Sith-Generation Computer Technology Series (Wiley-Interscience, New York, 1995)
33. C. Amiot, O. Dulieu, J. Chem. Phys. **117** (2002)
34. Particle Data Group, Eur. Phys. J. C **15**, 1 (2000); see also `http://pdg.lbl.gov/2002/statrpp.pdf`
35. A. Stuart, K. Ord, S. Arnold, *Classical inference and the linear model*, Kendall's advanced theory of statistics (Arnold, London, 1999)
36. T. Weber, J. Herbig, M. Mark, H.-C. Nägerl, R. Grimm, Science **299**, 232 (2003)
37. C. Drag, B. Laburthe Tolra, B. T'Jampens, D. Comparat, M. Allegrini, A. Crubellier, P. Pillet, Phys. Rev. Lett. **85**, 1408 (2000)
38. M. Marinescu, A. Dalgarno, Z. Phys. D **36**, 239 (1996)
39. J. Söding, D. Guéry-Odelin, P. Desbiolles, G. Ferrari, J. Dalibard, Phys. Rev. Lett. **80**, 1869 (1998)
40. P.J. Leo, E. Tiesinga, P.S. Julienne, D.K. Walter, S. Kadlecek, T.G. Walker, Phys. Rev. Lett. **81**, 1389 (1998)
41. R.Wynar, R.S. Freeland, D.J. Han, C. Ryu, D.J. Heinzen, Science **287**, 1016 (2000)